WISSENSCHAFTLICH-TECHNISCHE BERICHTE
FZR-288
Februar 2000
ISSN 1437-322X

A. Gokhman, J. Böhmert and A. Ulbricht

Contribution to the Determination of Microstructural Parameters from Small Angle Scattering Experiments at Reactor Pressure Vessel Steels

Herausgeber:
FORSCHUNGSZENTRUM ROSSENDORF
Postfach 51 01 19
D-01314 Dresden
Telefon +49 351 26 00
Telefax +49 351 2 69 04 61
http://www.fz-rossendorf.de/

Als Manuskript gedruckt

FORSCHUNGSZENTRUM ROSSENDORF
WISSENSCHAFTLICH-TECHNISCHE BERICHTE
FZR-288
Februar 2000

A. Gokhman, J. Böhmert and A. Ulbricht

Contribution to the Determination of Microstructural Parameters from Small Angle Scattering Experiments at Reactor Pressure Vessel Steels

The report bases on a project of the German Ukrainian Bilateral Cooperation in Science and Technology (UKR-004-98) funded by BMBF.
The authors appreciate the financial support.

Contents

Abstract:

Usually, the microstructure cannot be absolutely surely reconstructed from the small angle scattering pattern produced by it. The small angle neutron scattering curves measured at four C-poor ternary iron alloys were used to demonstrate the effect of the analysis method and the applied assumption on the microstructure analysis. Apart from the mean size of the scatterer, the size distribution as well as the shape of the scatterer affect the results. As a consequence, even well-proved methods as the indirect transformation method developed by Glatter can fail. The application of additional evaluation procedures or the use of information obtained by non-small angle scattering methods increases the chance to derive plausible structure models. In the paper a fit two-parameter method, the ratio between nuclear and magnetic scattering cross section and results from atom probe field ion microscopy are used for that. In this way it is shown that one of the four alloys exhibits another type of irradiation defects. Furthermore, modelling of the mechanical behaviours can also be helpful.

Zusammenfassung:

Aus dem Streubild im Kleinwinkelstreubereich kann im allgemeinen die die Streuverteilung erzeugende Struktur nicht eindeutig rekonstruiert werden. Anhand der Neutronen-Streubilder, die an vier C-armen ternären Fe-Legierungen aufgenommen worden waren, werden die Einflüsse des Analyseverfahrens und der der Analyse zugrunde gelegten Annahmen diskutiert. Von großem Einfluss auf die Streuwinkelabhängigkeit der Streuintensität ist nicht nur die mittlere Größe der streuenden Strukturinhomogenitäten, sondern auch ihre Größenverteilung und die Form der Streuer. Selbst ein gut bewährtes Verfahren zur Bestimmung von Teilchengrößenverteilungen, wie die indirekte Transformationsmethode nach Glatter, kann Fehlinterpretationen nicht ausschließen. Die Verwendung von anderen Auswertmethoden oder von Informationen aus Nicht-Kleinwinkelstreuuntersuchungen kann jedoch sehr hilfreich sein, plausible Strukturmodelle abzuleiten. Im gegebenen Beispiel werden dazu eine Fit-2-Parameter-Methode, das Verhältnis zwischen nuklearer und magnetischer Streuung sowie Ergebnisse von Atomsonden-Feldionenmikroskopie benutzt und für eine der untersuchten Legierung eine andere Defektstruktur abgleitet. Darüber hinaus können Modellrechnungen zum mechanischen Verhalten nützlich sein.

1 Introduction

The assurance of the mechanical integrity of the pressure vessel of a nuclear reactor (RPV) is an essential issue of safety. A main hazardous factor is the embrittlement caused by neutron radiation during operation. The phenomenon known as irradiation or neutron embrittlement depends on material aspects and irradiation conditions. It is specially critical for VVER-type reactors and limits the service life of these reactors. There are already numerous studies about the effect of material and irradiation parameters such as material composition, heat treatment, neutron fluence, neutron flux or irradiation temperature but the fundamental understanding of the phenomenon has not yet been developed sufficiently. Better understanding needs above all a thorough knowledge of the microstructural evolution due to irradiation.

The objective certainly is not trivial. First, RPV steel is a multi-component, multi-phase system consisting of different structural constituents and characterized by a strongly developed hierarchy of the structural appearances. The last includes as imperfections on the nanometre level as the prior-austenite grains with a size of about 100 µm. Second, RPVs are forged thick-walled components. Their microstructure is usually very heterogeneous. Finally, the typical irradiation-induced microstructural defects probably a) have nanoscale or even subnanoscale dimensions, b) differ in their nature, and c) are diffuse regarding their composition, structure and interfaces to the matrix. Therefore, even the experimental evidence is difficult and proven methods like transmission electron microscopy do not detect microstructural features although the mechanical properties already clearly show irradiation-caused changes.

Small angle neutron scattering (SANS) has proven to be useful in this field [1-28]. However, in contrast to the transmission electron microscopy, SANS does not provide an image of the microstructure in real space. Typically, SANS measures the spatial correlations of the scattering length density (or the electron density in the case of X-ray scattering) averaged over the sample volume and the measuring time for structural features with characteristic length of the order of 1 to hundreds of nanometres. That implies two peculiarities. On the one hand, SANS gives information not over individual features but average values what is often better appropriate to describe the response of a material. This is particularly advantageous in the case of the RPV steels because of their inhomogeneous structure. On the other hand, SANS does not allow to reconstruct the details of the microstructure which causes the scattering pattern. In particular for complex materials like RPV steel, large effort is necessary to gain microstructural data from the measured scattering intensity pattern. Apart from well-designed SANS experiments and careful data processing and data correction, additional information from other methods of the structure analysis must be involved. Above all it needs well-developed, sophisticated tools for analyzing the scattering pattern. For instances, in the case of a dilute system of polydisperse particles of identical form, there are several methods to estimate the size distribution function for the number or the volume of the particle [13,19,29-33]. Furthermore the ratio between the nuclear and the magnetic scattering provides additional information about the composition of the microstructural features [34]. As shown by Grosse et al. [35] this ratio can also be useful in the case of a system with homogeneous matrix and two different types of particles if one considers the dependence of the ratio on the particle size.

The Institute for Safety Research at Forschungszentrum Rossendorf e.V. has been concerned with SANS and SAXS studies of irradiated VVER-type RPV steels for several years. To support this work the experimental investigations have been complemented by numerical simulations of scattering pattern on the base of hypothetical models within a scientific cooperation with the South Ukrainian Pedagogical University Odessa. The following paper presents some results of joint works. First, a new procedure to determine the size distribution function is shown and compared with the Glatter method [30]. Then, the influence of the particle shape is investigated and the ratio between nuclear and magnetic scattering is evaluated. Finally, the irradiation hardening is estimated by means of the microstructural parameters determined by SANS. For this study, SANS results measured at ternary iron alloys were used.

2 Experimental data base

The following approaches bases on the SANS investigations at C-poor Fe alloys with different contents of Cu, P and Ni. All three elements are considered particularly harmful to irradiation embrittlement. The alloys are neither in the composition nor in the microstructure comparable with typical RPV steels. The microstructure is ferritic and, thus, the structure analysis is expected to be simpler rather than in case of the RPV steels.

The chemical composition and the final heat treatment are given in table 1.

Tensile and Charpy V-notched specimens were irradiated at the surveillance position of the VVER-440 reactors ROVNO 1 and KOLA 3 during one reactor cycle. Both reactor differ in the core design and so in the neutron flux (KOLA 3: $4.0 \cdot 10^{11}$n/cm², ROVNO 1: $3.0 \cdot 10^{12}$ n/cm² [$E_n > 0.5$ MeV]). Fluences of $F_1 = 1 \cdot 10^{19}$ and $F_2 = 8 \cdot 10^{19}$ n/cm² [$E_n > 0.5$ MeV] were reached. The irradiation temperature was about 270 °C.

The specimens were tested by Charpy impact testing and tensile testing. Details of the tests and the results are presented in [36].

The SANS experiments were carried out at the BENSC of Hahn-Meitner Institute (HMI) Berlin on the V4 spectrometer and at the PAXE facility of Laboratoire Leo Brillouin (LLB) Saclay under saturating magnetic fields of 1.4 T or 1.3 T respectively. As the experience has shown that for a qualified analysis of the SANS curves the scattering intensity must be measured over a sufficiently large measuring range, the experiments were performed with two different sample-detector distances. The experimental details are summarized in table 2.

For the data processing (correction of the detector sensitivity, background correction, separation of nuclear and magnetic scattering, calibration to the macroscopic scattering section) the local software routines were used. The background was corrected by measuring the scattering intensity of the empty sample holder. The transmission coefficient was experimentally determined. The absolute values were calibrated by means of a water standard at HMI and of a reference sample which was first calibrated at HMI for the experiments at LLB.

The separation of the magnetic and nuclear scattering is performed differently at both equipments. Whereas the HMI software uses all data of the detector and separates the magnetic and nuclear scattering by using the sinα dependence of the radially averaged counts, the LBB software takes only the detector data from the angle sector of ± 10° of the direction parallel and perpendicular to the magnetic field.

Table 1
Chemical composition and final heat treatment of the tested alloys

Code	Chemical composition, in wt-%, balance Fe						
	C	S	Cu	P	Ni	Si	Mn
A	0.01	0.004	0.015	0.002	0.01	0.15	0.39
B	0.01	0.005	0.42	0.012	0.01	0.24	0.49
C	0.01	0.004	0.12	0.010	1.98	0.09	0.35
D	0.01	0.004	0.12	0.012	1.10	0.12	0.41
E	0.01	0.004	0.12	0.039	1.13	0.20	0.46
F	0.01	0.004	0.42	0.012	1.19	0.21	0.47
G	0.01	0.004	0.11	0.013	0.012	0.37	0.48
H	0.01	0.004	0.11	0.039	0.010	0.24	0.49

Final heat treatments
Austenitizing: 980 - 1000 °C, oil-quenching
followed by a heat treatment of 10 h at 650 - 670 °C, air-cooling.

Table 2
SANS experimental conditions

	SANS-V4 (HMI/BENSC) Configuration		PAXE (LLB) Configuration	
	1	2	1	2
Detector type	$^{3}He(n,\alpha)$		$^{10}B_3F(n,\alpha)^{7}Li$	
Wavelength [nm]	0.5	0.5	0.5	0.6
Collimation length [m]	1.0	4.0	1.5	5.0
Distance sample-detector [m]	1.0	4.0	1.5	5.0
Q-range [nm]	0.1 - 3.2		0.06 - 2.5	
Magnetic field [T]	1.4		1.3	

3 Determination of size distribution function

3.1 The indirect transformation method (Glatter method)

For a dilute system of particles embedded in a homogeneous matrix and under the condition of magnetic saturation, the macroscopic neutron scattering cross section can be approximately described by the integral [37]

$$\left(\frac{d\Sigma(Q)}{d\Omega}\right)_{nuc} = \int_0^\infty D_v(R)\ \Delta\eta_{nuc}^2 \cdot K \cdot R^3 \cdot \phi(Q,R)\ dR, \qquad (1a)$$

$$\left(\frac{d\Sigma(Q)}{d\Omega}\right)_{mag} = \int_0^\infty D_v(R) \cdot \Delta\eta_{mag}^2 \cdot \sin^2\alpha \cdot K \cdot R^3 \cdot \Phi(Q,R)\ dR. \qquad (1b)$$

$\left(\frac{d\Sigma(Q)}{d\Omega}\right)_{nuc}$ and $\left(\frac{d\Sigma(Q)}{d\Omega}\right)_{mag}$ are the nuclear or magnetic contribution of the macroscopic SANS cross section, k is a constant depending on the shape of the particles, D_v is the volume distribution function and R is the characteristic dimension of the particles. $\Delta\eta$ is the difference between the mean scattering length densities of the particles and of the matrix and is given by

$$\Delta\eta = n_P \cdot b_P - n_M \cdot b_M\ . \qquad (2)$$

$n_{P,M}$ are the mean number densities of atoms and $b_{P,M}$ the mean scattering length in the particles or matrix, respectively. The so-called shape factor $\Phi(Q,R)$ is the Fourier transform of the shape of the particles. α is the angle between the magnetization vector of the sample and the scattering vector Q.

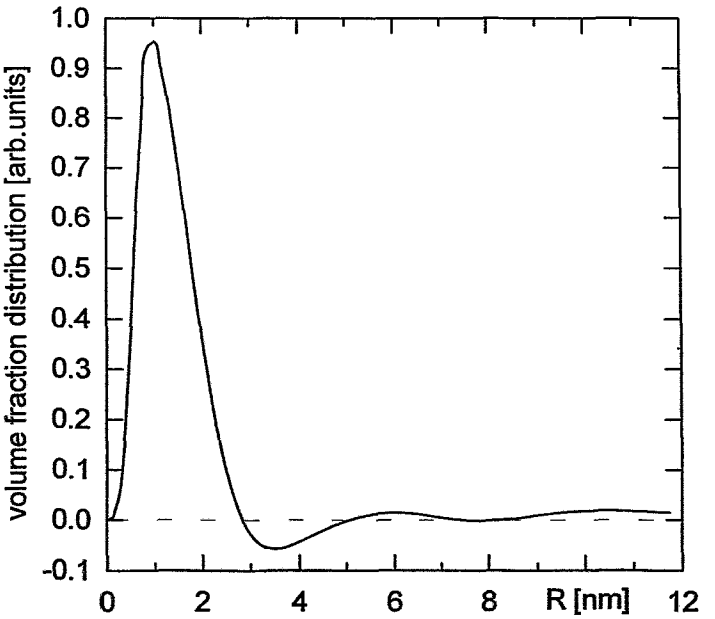

Fig. 1: Volume fraction distribution function with negative fraction computed by ITP92 without damping parameter.

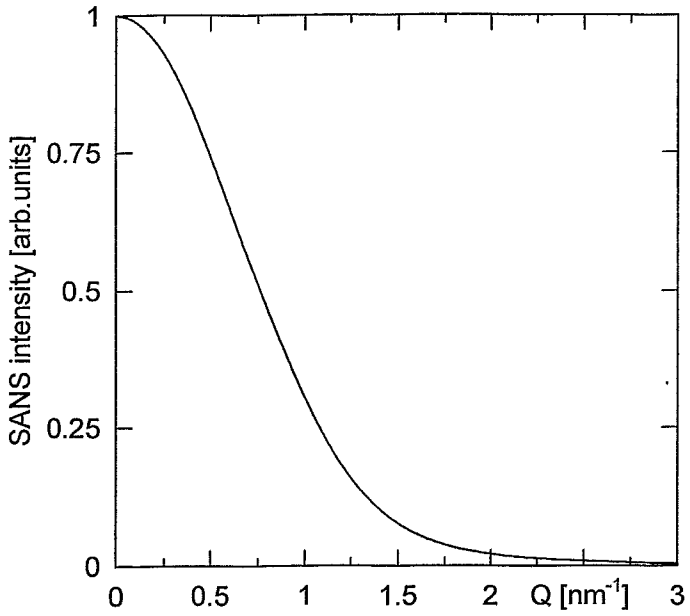

Fig. 2: Definition of a hypothetic SANS intensity curve.

Eq.(1) is the Fredholm-integral of the first kind. An approximated solution of the integral is given by Glatter [30] applying constrained weighted last-squares techniques for parameter estimation (called the indirect transformation method). The method assumes a) all particles have the same shape, b) the shape is a priori known, and c) the size distribution depends only on one linear size parameter *R*. The computer software "ITP-92" realizes all necessary computations.

The computation starts from the unsmoothed smeared experimental data. The error of the SANS data can result in size distribution functions which oscillate or have physically absurd negative fractions. An example of such an appearance shows Fig.1. SANS intensity is weak for the example, especially for the unirradiated and the post-irradiation annealed state, and, thus, the experimental error is relatively high. The oscillations of the course of the size distribution function certainly are not real.

To decrease this effect, the procedure contains a free damping parameter λ. The selection of the λ influences the size distribution function. However, there is no accurate algorithm to select the parameter λ in the damping procedure.

The influence of λ on the mean value of the particle size R and the volume fraction c_v calculated from the size distribution function was investigated. For this purpose an hypothetic SANS intensity curve, presented in Fig. 2, was defined and the size distribution function was computed by ITP 92 software using varied λ in the range from 0 till 4.0 with steps of 0.5. The results are depicted in Fig. 3. λ changes the position and the height of the maximum as well as the shape of the size distribution function. The oscillations decrease with increasing λ. The volume fraction c_v of the scattering particles is fluctuated between +/- 15 % and the change of the mean particle size R_{mean} is lower than 8 % within the tested range of values (Fig. 4). This shows that the results of the Glatter procedure are not very sensitive to λ.

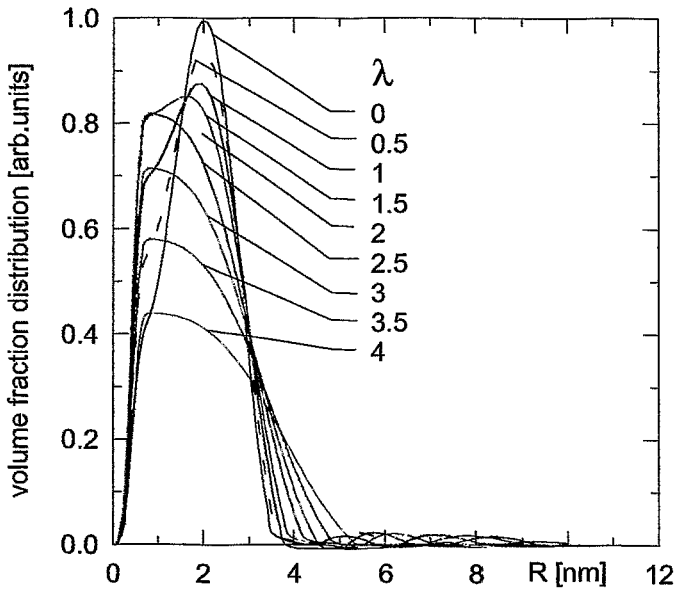

Fig. 3: Volume fraction distribution function computed from data of Fig. 2 by ITP92 with different damping parameter λ.

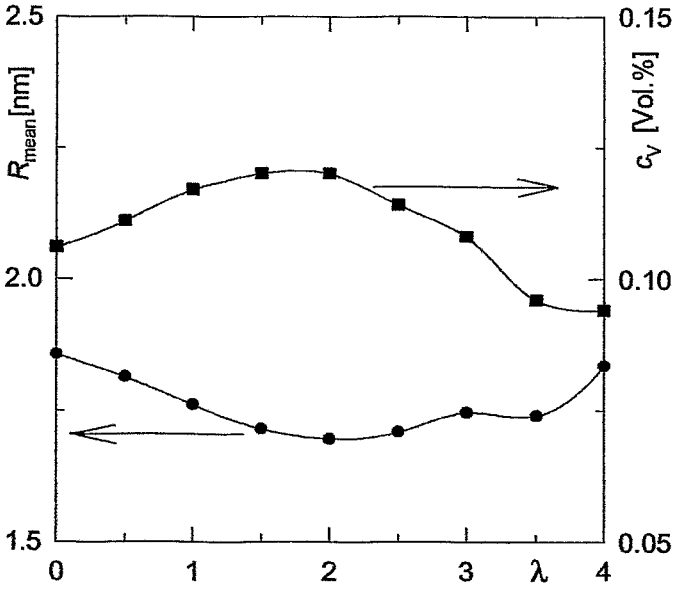

Fig. 4: Change of mean particle size R_{mean} and volume fraction c_V with the damping parameter.

3.2 A fit two-parameter method

The Glatter method is a more general approximation method. The integral equation (1) can also approximately solved by a fit parameter method assuming a known size distribution function with unknown fit parameters. The type of the size distribution function is selected on the base of a-prior information about the system. Then, the fit parameters are computed from the condition of the minimal divergence of the experimental data and the calculated data by the method of least squares.

For the following application it is assumed, first that the size distribution function of the scattering particles is described by a log-normal distribution characterized by the mode radius R_o and radius distribution parameter σ and, second, there are two types of scattering particles, which can differ in size and shape. The first assumption is a typical experimental finding in metallic systems [38], the second one is often observed as already mentioned.

The parameter of both size distribution function R_{01}, σ_1 and R_{02}, σ_2 can be found from the condition

$$\Delta = \left[\sum_{i=1}^{N} \left(\left(\frac{d\Sigma}{d\Omega}(Q_i) \right)^{exp.} - \left(\frac{d\Sigma}{d\Omega}(Q_i) \right)^{calc} \Big/ \mathrm{Er}(Q_i) \right)^2 \right]^{1/2} / N \rightarrow 0 \qquad (3)$$

by considering the dependence on the relative experimental error Er(Q). N is the number of experimental points.

The size distribution function is found from condition Eq.(3) by using the direct calculation of Δ in Eq.(3) under simultaneous change of all fit parameter in such manner that a global minimum of Δ is produced. The computer simulation will be recognized as successful if the value of the global minimum of Δ is found to be less than the estimation of the experimental error. Therefore, the method is only applicable if the experimental error is not too high ($\leq$ 8 %). The main characteristic of the approach used is the application of the direct way to find the minimal value of Δ in Eq.(3) (not the standard methods of non-linear programming).

More detailled, in Eq.(1) $D_v(R)$ is replaced by two log-normal functions

$$D_{v1}(R) = c_{v1} \cdot D^n_{v1}(R) \qquad (4a)$$

$$D_{v2}(R) = c_{v2} \cdot D^n_{v2}(R) \; . \qquad (4b)$$

c_{v1}, c_{v2} are the volume fraction of the type 1 and 2 of particles, $D^n_{v1}(R)$, $D^n_{v2}(R)$ are the log normal functions normalized by 1 with the parameters (R_{01}, σ_1) and (R_{02}, σ_2), respectively.

$$D^n_{v1}(R) = \frac{1}{\sqrt{2\pi}} \cdot \frac{1}{R \cdot \sigma_1} \cdot \exp\left[-\left(\ln \frac{R}{R_{01}} \right) \Big/ \left(2 \cdot \sigma_1 \right)^2 \right] \qquad (5a)$$

$$D^n_{v2}(R) = \frac{1}{\sqrt{2\pi}} \cdot \frac{1}{R \cdot \sigma_2} \cdot \exp\left[-\left(\ln \frac{R}{R_{02}} \right) \Big/ \left(2 \cdot \sigma_2 \right)^2 \right] . \qquad (5b)$$

For the calculation of the fit parameters, only the nuclear contribution of the SANS intensity in (1) was used. The reason is that the experimental error of the nuclear SANS cross section is lower than the error of the magnetic one.

Then, from (1a) it follows

$$\left(\frac{d\Sigma}{d\Omega}\right)_{nuc} = \Delta\eta_{mag}^2 \cdot \left(\frac{K}{A_1 - 1}\right) \cdot \int_0^{R_{max}} \left(D_{v1}(R) + X \cdot D_{v2}(R)\right) \cdot R^3 \cdot \Phi(R, Q)\, dR \qquad (6a)$$

or in the special case of spherical particles, respectively

$$\left(\frac{d\Sigma}{d\Omega}\right)_{nuc} = \Delta\eta_{mag}^2 \cdot \left(\frac{4\pi}{3}\right) \cdot \left(\frac{1}{A_1 - 1}\right) \cdot \left(\frac{1}{Q^6}\right) \cdot \int_0^{R_{max}} \left(D_{v1}(R) + X \cdot D_{v2}(R)\right) \cdot 9 \cdot \left[\sin(Q \cdot R) - Q \cdot R \cdot \cos(QR)\right]^2 \cdot \frac{1}{R^3}\, dR \qquad (6b)$$

with

$$X = \frac{A_1 - 1}{A_2 - 1} \quad . \qquad (7)$$

A_1 and A_2 are the ratio of the total SANS cross section to the nuclear cross section of the type 1 or 2, respectively, of the particles. Under the assumption of non-magnetic particles in a magnetic matrix, $\Delta\eta$ can be calculated as the magnetic scattering length of Fe:

$$\Delta\eta_{mag} = \eta_{mag}^{Fe} = 4.98 \cdot 10^{10}\ cm^{-2} \quad .$$

The programme FPM-99 to find the parameters R_{01}, R_{02}, σ_1, σ_2, c_{v1}, c_{v2} from Eqs.(3) - (7) and to compute the mean values of R for both types of particles and the total mean values of R is worked out on FORTRAN for IBM-PCI. Experimental nuclear SANS cross section and the experimental error in dependence of Q are input data of the procedure. Each experimental error has an own statistical weight that is inverse proportional to the experimental relative error of the data point. The programme does not work if the experimental error is higher than 8 %. Thus, the Q-range that is used for calculation is limited (usually: 0.273 .. 2.56 nm^{-1}).

The A-ratio of both types of particles in Eq.(6) is calculated from the experimental SANS data. First, the fit parameter of the normalized log normal function and the volume fraction of each particle type are computed from condition Eq.(3) as the result of the direct calculation of Eq.(3) with simultaneous change of the fit parameter in steps of 0.01 nm. Then, the total volume content and mean values of R of all particles are calculated.

Input and output data as well as the text of programme are described in the annex: „Description of the programme system FPM-99".

In comparison with the Glatter procedure, the fit two-parameter programme FPM-99 has the advantage to be applicable for a system with two-types of particles embedded in a matrix without restricting the shape of particles. However, it pre-defines the size distribution function and needs a relatively short interval of the possible values of the fit parameters.

Table 3
Structural paramter of the Fe alloys determined by the fit-two-parameter method for spherical particles

Alloy	R_{01} nm	σ_1	R_{02} nm	σ_2	$R_{1\,mean}$ nm	$R_{2\,mean}$ nm	c_{v1} %	c_{v2} %	Δ_{min} %
A, F_1	0.660	0.71			0.849		0.066		0.0299
A, F_2	0.925	0.575			1.091		0.20		0.0435
B, F_1	1.200	0.60	6.50	0.60	1.435	5.201	0.307	0.027	0.044
B, F_2	1.500	0.575	6.05	0.90	1.766	4.820	0.266	0.063	0.041
G, F_2	0.750	0.75	10.6	0.55	0.995	7.154	0.157	0.023	0.082
H, F_2	0.905	0.60	10.5	0.90	1.083	5.813	0.058	0.005	0.046

Table 4
Volume content c_v and mean radius R of the Fe alloys, Results of the Glatter method

alloy	A	B	G	H	A	B	A	B	G	H
state	unirradiated				F_1		F_2			
R [nm]					1.286	1.757	1.371	1.817	2.881	3.264
c_v [%]	0.002	0.02	0.008	0.014	0.053	0.71	0.22	0.71	0.16	0.11

Assuming spherical particles, the size distribution function was calculated by the fit-two-parameter method for the test alloys and compared with the Glatter procedure. Figs. 5a-f show the size distributions. In Figs. 6a-f the SANS intensity curves re-computed from the size distribution according to the Glatter procedure and the fit parameter method are depicted together with the experimental data. The main parameter are summarized in table 3. For comparison the results of the Glatter methods are given in table 4.

In general, similar trends are found with both methods. This concerns both the first strong maximum near $R \approx 1$ nm and the ranking of the different alloys and states. In detail, however, there are considerable differences. For example, the radius at maximum is usually smaller, the volume fraction of the particles is clearly lower in the case of alloy B, and the content of particles with higher radius is hardly indicated if one uses the fit parameter method.

As Figs. 6a-f show, the quality of the approximation is comparable for both methods, in the case of alloy A, irradiated to F_2 even better for the fit parameter method. However it must be considered the Q range which is used for the convolution is smaller for the fit parameter method than for the Glatter method. That means the information about the larger particles, which is concentrated at small Q values, is completely or at least partly got lost and the information about the approximately 1 nm particles, which is contained over a broad Q range, is reduced. This results in the loss of the fraction of particles with a larger radius and produces a narrow size distribution in the 1 nm-range.

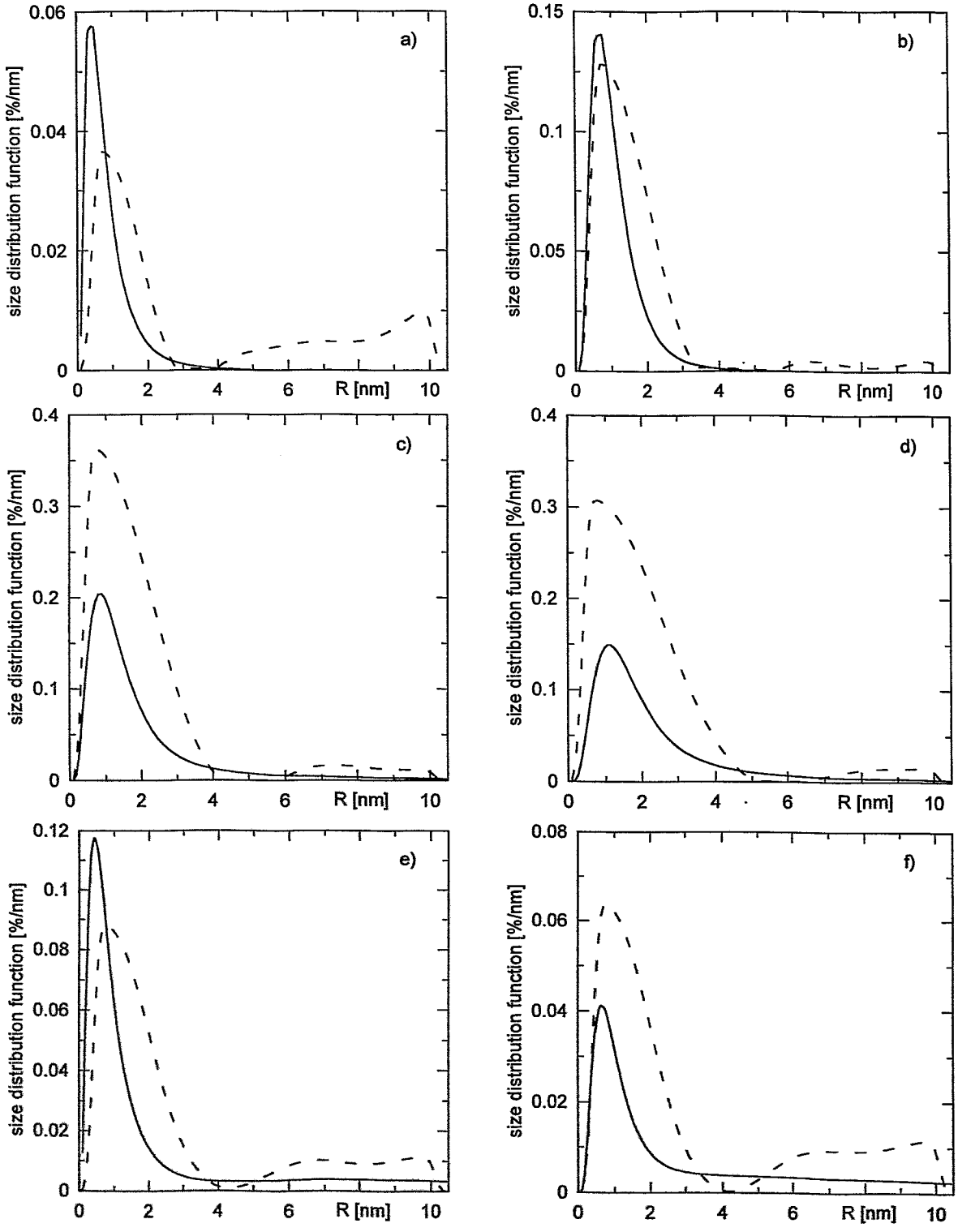

Fig. 5a-f: Size distribution function calculated by fit two parameter method (full line) and Glatter procedure (broken line) of the irradiated states of a) alloy A, F_1, b) alloy A, F_2, c) alloy B, F_1, d) alloy B, F_2, e) alloy G, F_2 and f) alloy H, F_2.

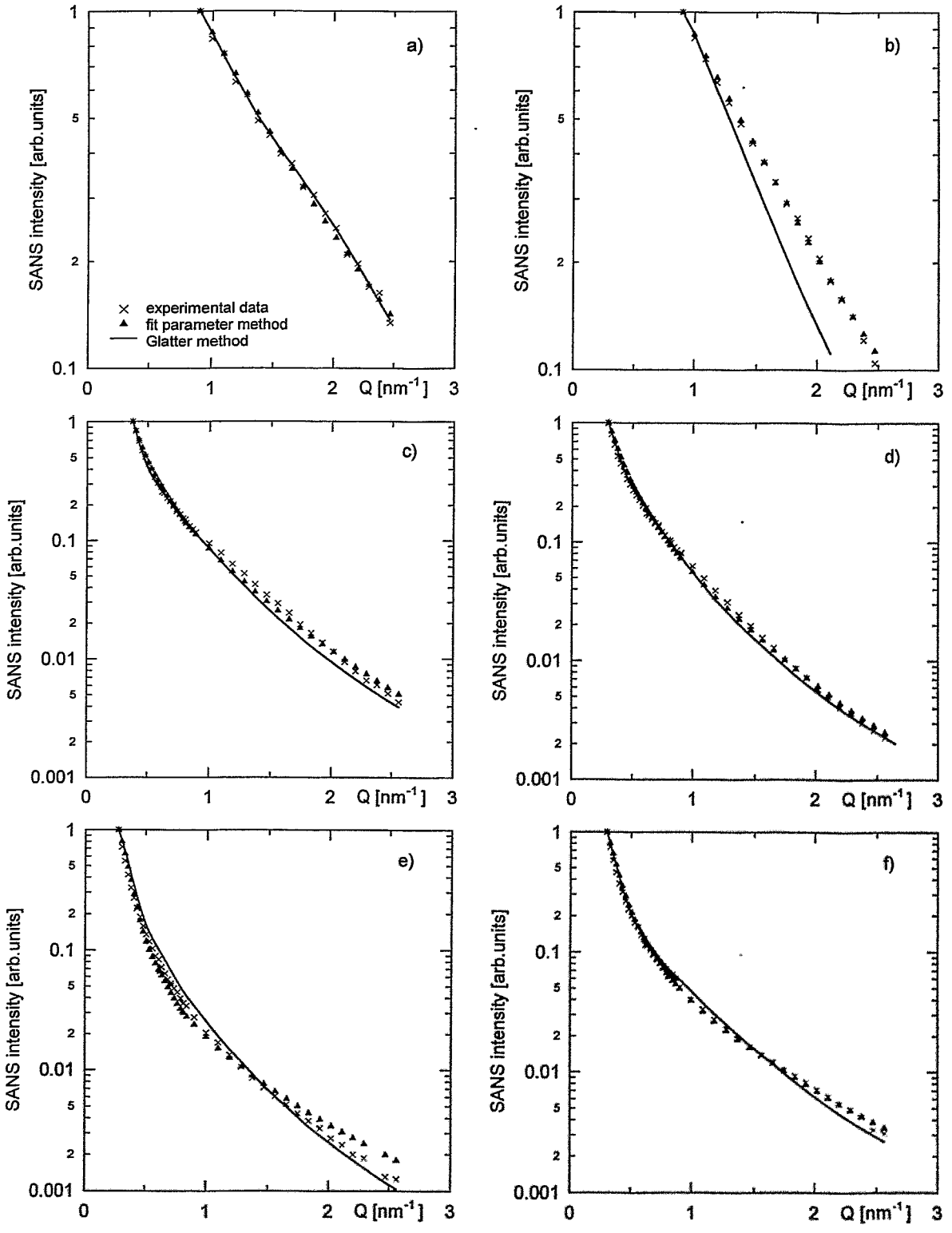

Fig. 6a-f: SANS intensities recomputed from size distribution functions of Fig. 5 and the experimental data of a) alloy A, F_1, b) alloy A, F_2, c) alloy B, F_1, d) alloy B, F_2, e) alloy G, F_2 and f) alloy H, F_2.

4 Influence of the shape of particles

There is hardly information about the shape of the irradiation-induced structure defects. Usually spherical shape is presumed. On the other hand, the RPV steel contains different carbides of plate-like, cube-like or rod-like shape. From other alloy systems it is known that early stages of decomposition produce flat inhomogenities which are thick only one or few atomic layer [39].

The influence of the spherical, rod-like and flat shape of the scatterers (particles) on the SANS intensity is tested for a given model distribution function with maximum at R= 2 nm.

Varying Eq.(1) SANS intensity can approximately be calculated from the scattering intensity of one single particle $I_1(Q,R)$ and the number of the particles $N(R)$

$$I(Q) = \frac{1}{V_s} \cdot \int_0^\infty I_1(Q,R) \cdot N(R)\, dR \ . \tag{8}$$

V_s is the volume of sample. $N(R) = V_P/V_1(R)$, where $V_1(R)$ is the volume of one particle, V_P the total volume of all particles. Considering

$$D_V(R) = \frac{V(R)}{V_s} \tag{9}$$

$I(Q)$ is given by

$$I(Q) = \int_0^\infty \frac{D_V(R) \cdot I_1(Q,R)}{V_1(R)}\, dR. \tag{10}$$

The scattering intensity of one particle $I_1(Q,R)$ does not only depend on Q and R but also on the shape of the particle. For a spherical particle the exact solution [40] is

$$I_1(Q,R) = \Delta\eta^2 \cdot 9 \cdot \left[\left(\sin(Q\cdot R) - Q\cdot R\cdot\cos(Q\cdot R)\right)/\left(Q\cdot R\right)^3\right]^2 \cdot V_1^2(R) \ . \tag{11}$$

$\Delta\eta$ is the magnetic or nuclear scattering contrast.

The Kratky and Porod approach has been used as a rule to obtain the $I_1(Q,R)$ for a rod-like and flat particle. Assuming that the rod makes a contribution to the diffraction only when it lies nearly perpendicular to scattering vector Q, the following formula can be derived for $I_1(Q,R)$:

$$I_1(Q,R) = \Delta\eta^2 \cdot \pi \cdot \frac{L}{Q} \cdot \left(\pi \cdot R^2\right)^2 \cdot \left[\frac{2 \cdot J_1(Q\cdot R)}{Q\cdot R}\right]^2 \ . \tag{12}$$

L is the length of rod; R is its radius and J_1 is the Bessel function of the first order. Eq.(12) is valid in case $L \gg R$.

In the same way for a flat particle the formula has been obtained:

$$I_1(Q,R) = \Delta\eta^2 \cdot 2 \cdot \left[\pi \cdot R \cdot \frac{T}{Q} \cdot \frac{\sin(Q\cdot T/2)}{Q\cdot T/2}\right]^2 \ . \tag{13}$$

T is the thickness of the flat particle. Eq.(13) is valid in the case of $T \ll R$ and under the assumption that the flat particle makes a contribution to the diffraction only when Q is nearly perpendicular to the plane.

After substitution of the Eq.(11-13) to Eq.(10) the following results for the scattering intensity $I(Q)$ is obtained:

For the system with spherical shape of particles:

$$I(Q) = \Delta\eta^2 \cdot \frac{4}{3} \cdot \pi \cdot \frac{1}{Q^6} \cdot \int_0^{R_{max}} \frac{D_v(R) \cdot 9 \cdot \left[\sin(Q \cdot R) - Q \cdot R \cdot \cos(Q \cdot R)\right]^2}{R^3} \, dR \qquad (14)$$

For the system with rod-like shape of particles:

$$I(Q) = \Delta\eta^2 \cdot \frac{\pi^2}{Q} \cdot \int_0^{R_{max}} D_v(R) \cdot \left[\frac{2 \cdot R \cdot J_1(Q \cdot R)}{Q \cdot R}\right]^2 dR \qquad (15)$$

For the system with flat shape of particles:

$$I(Q) = \Delta\eta^2 \cdot 2 \cdot \pi \cdot T \cdot \left[\frac{\sin(Q \cdot T/2)}{Q \cdot T/2}\right]^2 \cdot \frac{1}{Q^2} \cdot \int_0^{R_{max}} D_v(R) \, dR \, . \qquad (16)$$

SANS intensity functions, normalized to the intensity at the lower boundary of the measuring range of Q, versus Q for the given model size distribution function and different shapes of particles are shown in Fig. 7. The scattering curve strongly changes with the shape of particles.

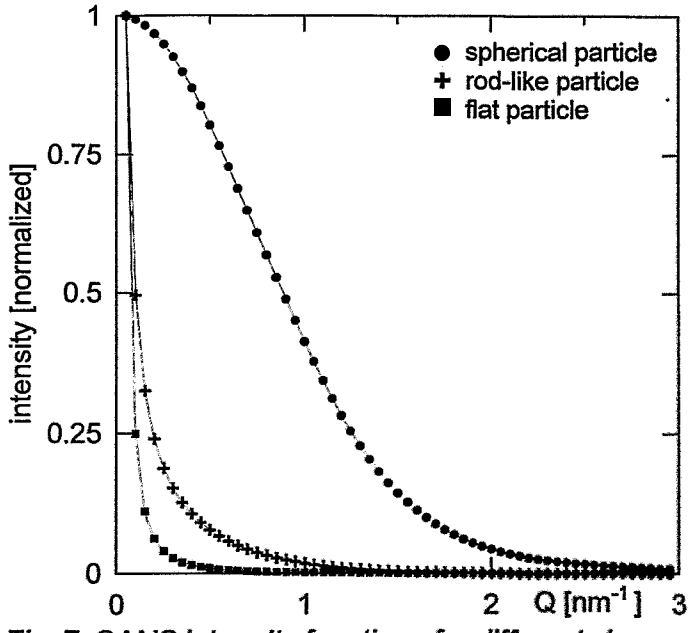

Fig. 7: SANS intensity functions for different shapes of particles.

Two conclusions are evident: a) a wrong assumption about the shape of particles results in a wrong size distribution function and b) the Glatter method fails for the case of a composite 2-particle type-matrix system if the two different types of particles also have different shapes.

Note that for the system of rod-like particles the SANS intensity does not depend on the length of the rods if the diameter is constant for all particles in this system according to the Eq.(15).

From analyses of Eq.(16) it is possible to conclude that in case of the flat particles with the same thickness the $I(Q)$ curves must be parallel for different thickness of them and the product

$$\Psi = I(Q)\cdot Q^2\cdot\left[\frac{Q\cdot T/2}{\sin(Q\cdot T/2)}\right]^2 \qquad (17)$$

does not depend on Q for such a system.

This result can be considered a criterion. If Ψ is constant over Q for each experimental value Q, the investigated structure contains flat particles with the same thickness.

The criterion is used for the SANS experiments at the test alloys A - H. Two examples are given in Fig. 8. Besides the Q dependence of the parameter Ψ, the experimental $I(Q)$ dependence are depicted together with the computed $I(Q)$-dependence by Eq.(16). For the last it was used the size distribution function which was determined before by the Glatter procedure and under the assumption of spherical particles. The intensity curves are again normalized to the intensity at the lower boundary of the measuring range. In every case the experimental and computed curves are not identical. This is not surprising and proves only the clear influence of the particle shape on the scattering pattern. As a more important result, an approximately constant course can only be noted for the very pure alloy A in both irradiated states (Fig. 8a). Since this alloy deviates from the appearances of the other alloys in other respects as well, this is considered as a hint that there special types of irradiation-induced defects are produced. All other alloys investigated do not show constant courses.

Transmission electron microscopy investigations provide the evidence of small cylindrical particles in VVER-type RPV steels [41]. As a further example of the effect of particle shape, a composite model of cylindrical and spherical particles is to be considered and to be used for analyzing of the SANS curves of the test alloys with the fit parameter method. As above mentioned, the Glatter procedure does not permit analyses in such cases.

It is presumed a system with cylindrical and spherical particles. The cylindrical particles are arbitrarily oriented relating to the scattering vector Q and have an arbitrary ratio of radius to length. In this case the vector Q can be resolved into a component Q_1 that is parallel to the axis of the cylinder, $Q_1 = Q\cdot y$ (y is the cosine between Q and Q_1), and a component Q_2, that is the perpendicular to one, $Q_2 = Q\cdot(1-y^2)^{0.5}$ (Fig. 9). Now the SANS intensity from the single cylinder can be described as an integral of the product of the SANS intensity from the scattering of the cylindric (Eq.(12)) and the axial section (Eq.(13)) over y:

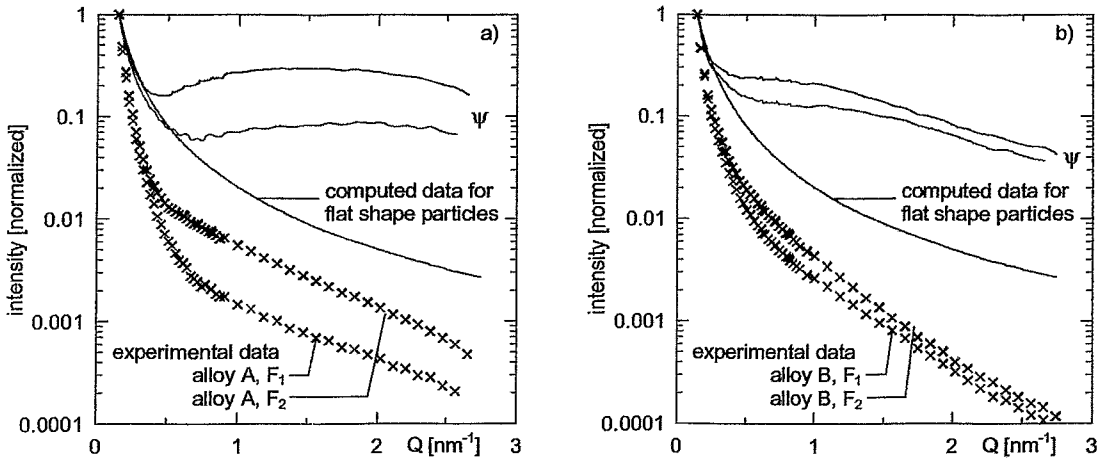

Fig. 8: Experimental data, computed scattering function for flat particles and flat particle criterion of a) alloy A, and b) alloy B.

$$I_1(Q,R) = \left(\Delta\eta \cdot T \cdot \pi \cdot R^2\right)^2 \cdot \mathrm{FF}(Q,R,T) \tag{18}$$

with

$$\mathrm{FF}(Q,R,T) = \int_0^1 \left[\frac{\sin(Q \cdot T \cdot y/2)}{Q \cdot T \cdot y/2}\right]^2 \cdot \left[\frac{2 \cdot J_1\left(Q \cdot R \cdot \sqrt{1-y^2}\right)}{Q \cdot R \cdot \sqrt{1-y^2}}\right]^2 \mathrm{d}y.$$

Substituting Eq.(18) in Eq.(8) the SANS intensity from a system with cylindric particles of the same thickness but different radius is obtained:

$$I(Q) = \Delta\eta^2 \cdot T \cdot \pi \cdot \int_0^{R_{max}} D_v(R) \cdot R^2 \cdot \mathrm{FF}(Q,R,T)\, \mathrm{d}R. \tag{19}$$

Substitution of Eq.(14) for the spherical shape system, Eqs.(4) and (5) for the log-normal size distribution function and Eq.(19) for the cylindrical shape system yields the nuclear contribution of the SANS intensity in the dependence on Q for the composite model of cylindrical and spherical particles

$$I(Q)_{nuc}^{calc} = \Delta\eta_{mag}^2 \cdot T \cdot \pi \cdot c_{v1} \cdot \frac{1}{A_1 - 1} \cdot \int_0^{R_{max}} D_{v1}^n(R) \cdot R^2 \cdot \mathrm{FF}(Q,R,T) + \mathrm{CX} \cdot D_{v2}^n(R) \cdot 9 \cdot \left[\frac{\sin(Q \cdot R) - Q \cdot R \cdot \cos(Q \cdot R)}{(Q \cdot R)^3}\right]^2 \cdot R^3 \, \mathrm{d}R. \tag{20}$$

$D^n_{v1}(R)$ and $D^n_{v2}(R)$ are the normalized log normal functions for cylindrical and spherical particles and

$$CX = \frac{c_{v2}}{c_{v1}} \cdot \frac{A_1 - 1}{A_2 - 1} \cdot \frac{4}{3 \cdot T} .$$

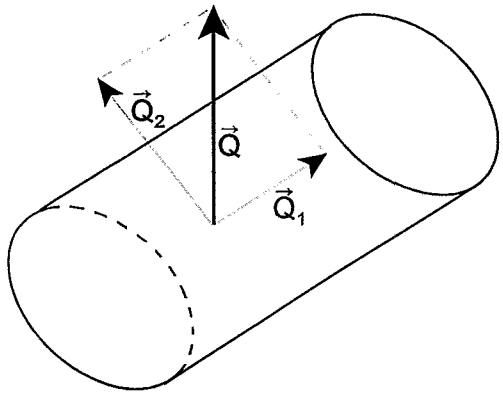

Fig. 9: Components of the scattering vector.

Using the programme FPM 99, the parameter R_{01}, σ_1, R_{1mean}, T, and c_{v1} of the cylindrical-shaped type of particles and the parameters R_{02}, σ_2 , R_{2mean}, and c_{v2} of the spherical one were computed for the test alloys in the irradiated state. The composite model does not provide a solution for the alloy B in both irradiated states. Values of microstructural parameters of the alloys A, G and H are given in table 5. Examples of the size distribution function are shown in Fig. 10. In Fig. 11 the re-computed SANS curves are compared with the experimental results and with the curves that were re-computed from the Glatter analysis.

Table 5
Microstructural parameters of the Fe alloys A, G and H using the fit parameters method and a composite model of cylindrical and spherical particles

alloy	R_{01} [nm]	σ_1	R_1 [nm]	T [nm]	R_{02} [nm]	σ_2	R_2 [nm]	c_{v1} %	c_{v2} %	Δ
A, F_1	1.3	2.5	1.224	1.35				0.0202		0.0244
A, F_2	1.06	1.05	1.628	1.58				0.039		0.0252
G, F_2	3.55	0.40	3.819	0.32	10.5	0.67	6.63	0.231	0.032	0.0639
H, F_2	0.31	1.50	0.858	0.39	10.5	1.6	4.15	0.164	0.055	0.0872

In comparison with the results of the spherical model computed by the fit parameter method (table 3), the error parameter Δ is lower for the composite model in the case of A,F_1; A, F_2 and G, F_2. The alloy A exhibit only one type of irradiation-induced defects that shape a kind of disc with $R = T$. Furthermore the comparison with the Glatter analysis also proves a better approximation of the experimental results by the model with cylindrical-shaped particles than the spherical model (Fig. 11b). Eventually, this corresponds to the above-mentioned result with the flat criterion. However, the composite model does not provide reasonable results for all other alloys investigated. The procedure is not applicable for alloy B and provides completely different results for the alloys G and H. There is no evidence for such difference from other experiments. Besides the re-computed SANS curves for the composite model and the Glatter analysis meet the experimental values with comparable scatters.

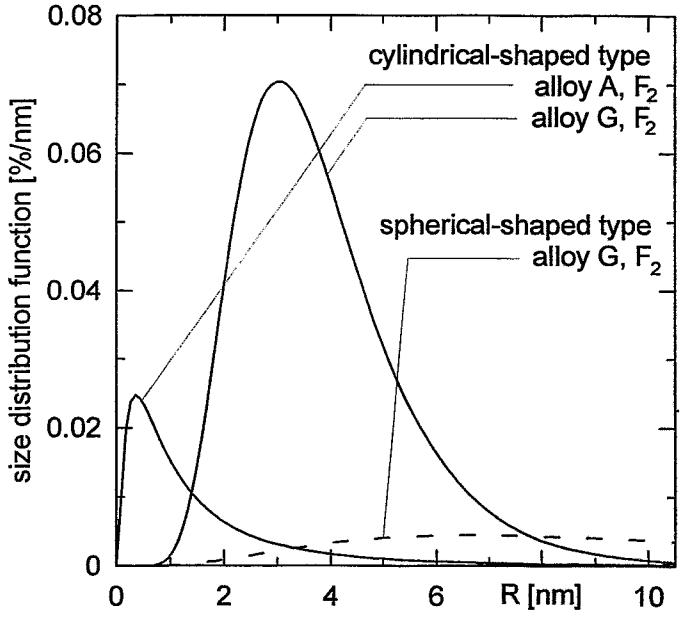

Fig. 10: Size distribution functions of cylindrical- and spherical-shaped type of particles.

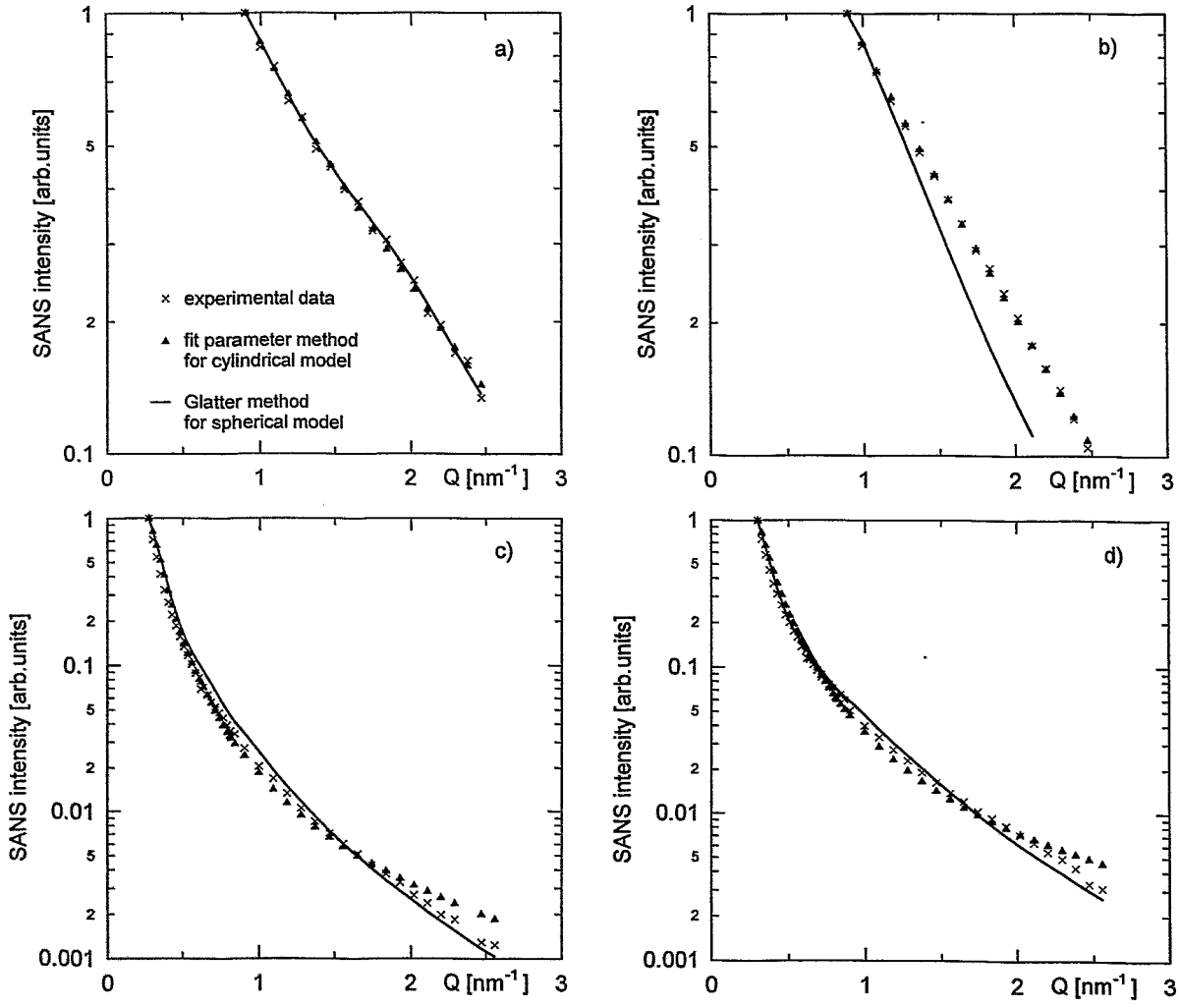

Fig. 11a-d: SANS intensities, recomputed from the results of the fit parameter method for a composite model and of the Glatter procedure for spherical particles, of a) alloy A, F_1, b) alloy A, F_2, c) alloy G, F_2, d) alloy H F_2.

5 Evaluation of the A-ratio

The differences between the magnetic and the nuclear SANS contrast can provide additional information about the composition and the structure of the scattering particles.

For this an often used parameter is the so-called A-ratio:

$$A = \frac{\left(\frac{d\Sigma(Q)}{d\Omega}\right)_{nuc} + \left(\frac{d\Sigma(Q)}{d\Omega}\right)_{mag}}{\left(\frac{d\Sigma(Q)}{d\Omega}\right)_{nuc}} . \qquad (21)$$

Unfortunately, its interpretation is not unambiguous and needs ad-hoc assumption or knowledge from other investigations.

The investigated Fe alloys show characteristic differences [42]. Whereas for the alloys with low Cu content the A-ratio is about 1.6 - 1.8, the Cu-rich alloys exhibit an A-ratio of 3 - 6.

The last seems to be caused by Cu-rich participitates. Such precipitates was investigated by atom probe field ion microscopy (APFIM) in VVER 440 weld metal after irradiation up to $3.5 \cdot 10^{19}$ n·cm^{-2} (E_n > 1 MeV) [43]. Although the material is clearly different of the investigated alloys in this paper, the results could be a suitable approach for the analysis of the A-ratio.

Table 6
Distribution of the foreign atoms in the cluster according to APFIM [42]

r [nm]	Fe [at. %]	Si [at. %]	Mn [at. %]	Ni [at. %]	Cu [at. %]	P [at. %]
0	54.2	6.25	12.0	10.0	18.0	0.0
0.5	71.0	6.0	8.0	5.0	15.0	0.0
1.0	79.4	3.75	7.0	4.0	7.0	0.0
1.5	87.5	3.0	3.0	2.0	2.0	2.0
2.0	98.0	0.0	0.0	0.0	0.0	2.0
2.5	100	0.0	0.0	0.0	0.0	0.0

Pareige et al. [43] observed cluster with a concentration profile over the radius of the cluster. The analysis of a cluster with a radius of 2 nm as function of the distance r from the cluster centre is given in table 6. The cluster contains the foreign atoms Si, Mn, Ni and Cu. Their concentration decreases with increasing distance r. P is only present in an outer shell. The content of the matrix element Fe increases with the distance. The method does not provide information about the content of vacancies and, thus, about the number density in the cluster.

The mentioned elements also are constituent of the tested alloy and the particle size determined by SANS is comparable. Thus, the use of the APFIM result from [43] seems to be justified.

Using the experimental A-ratio and the APFIM results the number density of the Cu-rich particles (clusters) can be calculated on the base of

$$A = 1 + \left[\frac{b_{Fe}^{mag}}{b_{Fe}^{nuc}} \cdot \left(c_{Fe} - \frac{1}{K} \right) \cdot \frac{1}{\sum_{x_i} c_{x_i} \cdot \left(\frac{b_{x_i}^{nuc}}{b_{x_i}^{mag}} - \frac{1}{K} \right)} \right]^2 \qquad (22)$$

c_{xi}, b_{xi}^{nuc} are the concentration and scattering lengh for nuclear SANS of the x_i foreign atom in cluster, b_{Fe}^{mag} is the scattering length for magnetic SANS of iron, and K is the ratio of particle density to the matrix (iron) density.

The result of the calculation of the density ratio as a function A-ratio is given in Fig.12. For the experimental values of 4.7 and 3.8 for alloy B irradiated to a fluence of $1 \cdot 10^{19}$ or $8 \cdot 10^{19}$ n/cm^2 [E_n > 0.5 MeV], respectively, the density ratio is about 1.02 to 1.035. This means that the Cu-rich precipitates have only a low content of vacancies in contrast to the often mentioned view in the literature.

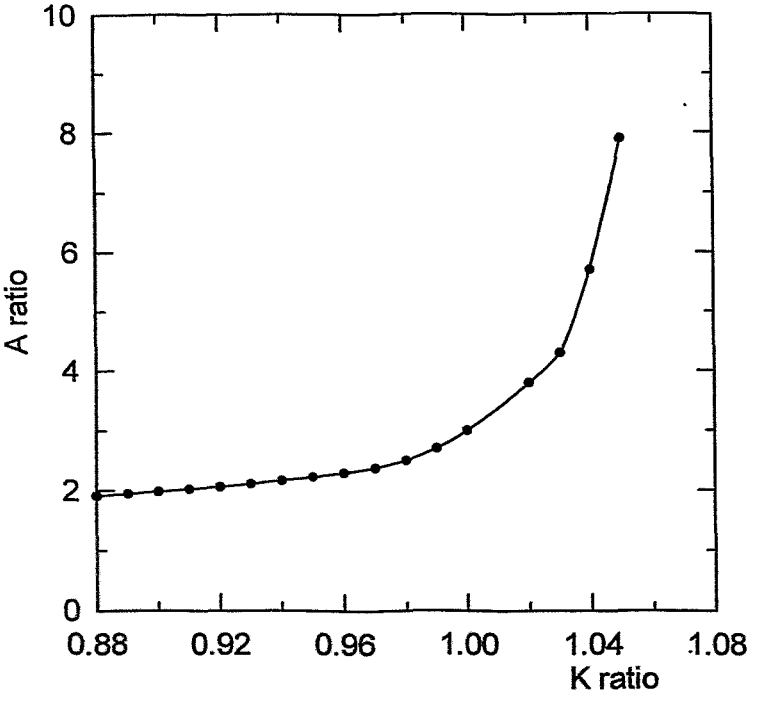

Fig. 12: A ratio as function of particle density ratio K.

Another model discussed often assumes irradiation-induced defects as complexes from Cu atoms and vacancies. For this case the minimal volume fraction of Cu in the complexes (V_{Cu}/V_{cl}) can be estimated from A-ratio.From Eq.(21) the minimal value is obtained:

$$c_{Cu_{min}} = \frac{b_{Fe}^{nuc}}{b_{Cu}^{nuc}} \left[1 \pm \frac{b_{Fe}^{nuc}}{b_{Cu}^{nuc}} \cdot \frac{1}{\sqrt{A-1}} \right]. \tag{23}$$

Considering

$$\left(\frac{V_{Cu}}{V_{cl}} \right)_{min} = c_{Cu_{min}} \cdot \frac{\rho_{Fe}}{\rho_{Cu}} \tag{24}$$

(ρ_{Fe} and ρ_{Cu} are the density of iron and copper respectively) from Eqs.(23,24) a Cu-concentration of 70 % is estimated. The result seems to be not unrealistic.

Thus, the A-ratio determined from the SANS experiments with the Fe alloy with high Cu content is consistent with both the model of vacancy-copper complexes and of iron-solutes cluster of the same density like the matrix.

6 Estimation of the Irradiation Strengthening

Hardening due to defect clusters or copper precipitates can be estimated by a dispersed barrier model. Often used approaches go back to Orowan [44], Friedel [45], Week et.al. [46], and Russel and Brown [47].

The Orowan model describes hardening due to hard particles with sufficiently large particle distances. In this case the dislocation is bent between the particles and passes them leaving a dislocation ring around each particles. The needed shear stress τ_0 is

$$\tau_0 = \alpha \cdot \frac{G \cdot b}{L}, \tag{25}$$

where G is the shear modulus, b is the magnitude of Burgers vector, L is the average barrier spacing and α is a constant. More generally, the relation can be extended by considering a polycrystalline matrix with randomly oriented grains and further potential interactions between dislocations and particles:

$$\Delta\sigma = 3.1 \cdot \frac{G \cdot b}{\beta \cdot L}. \tag{26}$$

β is the measure of the barrier strength. For small β the dislocation will shear the particle, in case of $\beta \approx 1$, the Orowan-looping mechanism is effective. Particularly the nanoscale irradiation defects are passed rather by cutting than by the Orowan mechanism.

The shear modulus of iron is estimated as $(8.81 \cdot 10^4 - 31 \cdot T)$ MPa [47, 49], where T is the temperature; and the Burgers vector b = 0.249 nm.

Estimates of β for small point defect clusters and interstitial loops in bcc materials range from 1.5 to 5.0. If interstitial loops are assumed to be strong barriers, b = 3-4 in the Orowan model. Recent measurements [48] of the tensile properties and detailed TEM examination of irradiated fcc copper indicated that for clusters with mean diameters below 3 nm β = 4.

The mean distances L is calculated from the number density N and mean diameter d of the obstacles:

$$L = \sqrt{N \cdot d} \; . \tag{27}$$

The Orowan mechanism provides an upper limit of the irradiation hardening.

The lower limit of the hardening due to point defects is estimated by the weak barrier model that incorporates Friedel's effective barrier spacing:

$$\Delta\sigma = 3.1 \cdot G \cdot b \cdot d \cdot \frac{N^{2/3}}{\beta}, \tag{28}$$

with β = 8 for bcc materials.

A model proposed by Weeks et al. [46] leads to values that are between the results of the Orowan and Friedel model.

For hardening due to copper rich precipitates the Russel - Brown model [47] is used. It differs from the other models in that the hardening arises from a difference between the shear modulus of the precipitates and shear modulus of the iron matrix [49]:

$$\Delta\sigma = 3.1 \cdot 0.8 \cdot G \cdot \frac{b}{L} \cdot \sqrt{1 - \frac{E_{ppt}}{E}} \; ; \; \sin^{-1}(E_{ppt}/E) < 50 ,$$

$$\Delta\sigma = 3.1 \cdot G \cdot \frac{b}{L} \cdot \left(1 - \frac{E_{ppt}}{E} \right)^{0.75} \; ; \; \sin^{-1}(E_{ppt}/E) > 50 , \tag{29}$$

where

$$\frac{E_{ppt}}{E} = \frac{1}{\ln\left(\frac{r_c}{r_0}\right)} \cdot \left[\frac{E^{\infty}_{ppt}}{E^{\infty}} \cdot \ln\left(\frac{r_{ppt}}{r_0}\right) + \ln\left(\frac{r_c}{r_{ppt}}\right) \right] . \tag{30}$$

The ratio $E_{ppt}^{\infty}/E^{\infty}$ in Eq.30 is equal to the ratio of the precipitates shear modulus to the matrix shear modulus if one neglects the difference of their Poisson coefficient values [49].

Stoller recommends to use $E_{ppt}^{\infty}/E^{\infty} = 0.6$ for copper-rich precipitates in iron matrix.

Other variables in Eq.(30) are r_{ppt}, the mean radius of the precipitate, $r_0 = 2 \cdot b$, the inner cut-off or dislocation core radius and r_c, the outer cut-off radius of dislocations.

Although Russel and Brown used $r_c = 1000 \cdot r_0$, such a value seems physically unreasonable for engineering materials since it is larger than the mean spacing of dislocations. More exactly to take this value as a just mean dislocation spacing:

$r_c = (\pi \cdot \rho_n)^{-0.5}$ where ρ_n is the network dislocation density [49].

The parameter L in Eq.(29) is the planar spacing between the equiaxial copper particles. It is possible to calculate L in terms of the volume content of precipitates in the following way [50]:

$$L = 1.77 \cdot \frac{r_{ppt}}{\sqrt{c_v}} \quad . \tag{31}$$

Irradiation hardening of the Fe alloys due to the point defect cluster is estimated by Eqs.(26) and (28) and due to the copper-rich defects is estimated by Eqs.(29-31) on the base of the parameters of damage structure that are calculated from SANS data by the Glatter method as well as by the fit parameter method for both a system with two types of spherically shaped particles and a composite (cylindrical and spherical) system. The mean diameter in Eqs.(26, 28) and the mean radius of precipitates in Eqs.(29-31) and c_v are taken from the data for first phase in the tables 3-5. The number density of precipitates is also calculated by means of c_v and mean R (R_1) of the first phase:

$$N = \frac{c_v}{V_1} \quad . \tag{32}$$

where $V_1 = (4 \cdot \pi/3) \cdot R_1^3$ for spherical phase and $V_1 = \pi \cdot R^2 \cdot T$ for cylindrical phase.

Estimation of the change in shear stress of the irradiated Fe-alloys in Orowan, Friedel and Russel-Brown approaches are given in table 7.

Table 7
Estimation of the change in shear stress (in MPa) of the irradiated Fe alloys in Orowan, Friedel and Russel-Brown approaches on the base of the parameters of damage structure that obtained from SANS data by Glatter method (GL), fit parameters method for spherical shape (FPS) and fit parameters method for cylindrical shape (FPC).

Sample	Orowan approach			Friedel approach			Russel-Brown approach		
	GL	FPS	FPC	GL	FPS	FPC	GL	FPS	FPC
A, F_1	195	276	250	27	53	17	127	179	80
A, F_2	373	384	264	65	93	21	250	296	92
B, F_1	640	333		137	93		383	327	
G, F_2	191	373	309	32	85	153	134	271	253
H, F_2	111	242	497	17	34	176	101	365	130

As expected the Orowan model yields the highest strengthening whereas the Friedel model shows the lowest effect in every case. On the other hand, there are considerable differences due to the different SANS evaluation procedures. The fit parameter method assuming cylindrally shaped particles provides results which are far from experimental results of mechanical tests for all investigated specimens apart from alloy A.

7 Conclusion

Experimental small angle neutron scattering curves measured at Fe alloys with different contents of Cu and P were used to investigate the effect of the evaluation procedure and of the assumptions taken as a basis for the evaluation. As a standard method for estimating size distribution of the scattering particles or structure defects, the indirect transformation method developed by Glatter has been proved. The Glatter procedure uses a free damping parameter to avoid oscillations of the size distribution function or negative portions. The selection of the damping parameter is quite arbitrary but does not considerably affect the integral parameters 'volume fraction' and 'mean diameter'. However, the shape of the scatterer must be assumed and the method fails for the case of two types of particles with different shapes.

Therefore, the additional analysis with another procedure of approximation can be useful. Without great effort a fit two-parameters method is suitable. In this case the size distribution function is assumed and the parameters of the function are estimated in such manner that the squares of deviations between experimental scattering intensity and calculated one are a minimum. The procedure can also applied for systems with more than one type of particles and the types can even have different shapes. On this base a FORTRAN programme for IBM-PC is designed. With this programme the experimental results are evaluated assuming spherical, cylindrical or plate-like particles and compared with the results of the Glatter procedure for spherically shaped particles. As the basis for the fit two-parameters approach a log-normal distribution seems to be appropriate. The calculations show that the shape of the particles affects strongly the results obtained. In principle, the following way leads to a structure model that is the most plausible one:

- Computing of the size distribution function for different systems (different shapes and different types of particles) and with different evaluation procedures (like Glatter or fit two-parameter method),
- Recomputing of the scattering curves from the size distribution function obtained by the first step,
- Comparison of the recomputed and experimental curves and determination of the deviation square.

The model that shows the least deviation square is most plausible. However, such decisions can only be made on basis of experimental results of very low error. This condition is not met in the rule. Progress promises the use of more sophisticated fit parameter methods which were developed for so-called ill-posed problems. They even provide reliable results in the case of high experimental error.

For flat particles with the same thickness a criterion that does not depend on the scattering vector can be derived. In one of the investigated cases (alloy A, irradiated) the criterion meets approximately the experimental results.

Additional information can be gained by the ratio between nuclear and magnetic scattering (in the paper modified as A-ratio). The A-ratio of alloy A differs clearly from the value of alloy B. Thus, both alloys certainly have different types of radiation defects.

For alloy B Cu-rich precipitates seems to appear. Using results from atom probe field ion microscopy the Cu content in the precipitates or their density can be estimated from the A-ratio measured. The result is consistent with a structure model consisting of precipitates with 70 % Cu and 30 % vacancies or of clusters formed by Fe, Cu and other foreign atoms with the same density as the matrix.

Eventually, the structural parameters obtained by the small angle scattering experiments can be used to estimate the irradiation strengthening. There are many approaches and, for the estimation, numerous parameters must be assumed. Therefore successful modeling needs repeatedly feedback between microstructural analysis, mechanical testing and model estimation to find reliable approaches.

References

[1] Frisius, F., M. Naraghi, Atomkernenergie 29 (1977) 139-144

[2] Little, E.A., „Strain Aging and Neutron Scattering Studies on Irradiated PWR Pressure Vessel Steels", in: Effects of Radiation on Materials: Twelfth International Symposium, ASTM STP 870, F.A. Garner, J.S. Perrin, Eds., 1985, pp. 1009-1026

[3] Buswell, J.T., E.A. Little, R.B. Jones, R.N. Sinclair, „Analysis of Microstructural Changes in Irradiated Pressure Vessel Steels Using Small Angle Neutron Scattering", Proc. of the Second International Symposium on Environmental Degradation of Materials in Nuclear Power Systems-Water Reactors, Montery, 1985, J.T.A. Roberts, J.R. Weeks, G. Thons, Eds., American Nuclear Society, 1986, p. 139

[4] Solt, G., F. Frisius, W.B. Waeber, „Defect Particles in an Irradiated RPV steel Studied by a Systematic Variation of Irradiation and Annealing Conditions: Preliminary Results by Small Angle Neutron Scattering", in: Radiation Embrittlement of Nuclear Reactor Pressure Vessel Steels: An International Review (Third Volume) ASTM STP 1011, L.E. Steele, Ed., 1989, pp. 229-242

[5] Beaven, P.A., F. Frisius, R. Kampmann, R. Wagner, J.R. Hawthorne, „SANS Investigations of Irradiated A 533-B Steels Doped with Phosphorus", in: Radiation Embrittlement of Nuclear Reactor Pressure Vessel Steels: An International Review (Third Volume) ASTM STP 1011, L.E. Steele, Ed., 1989, pp. 243-256

[6] Maury, F., N. Lorenzelli, C.H. DeNovion, J. Nucl. Mater. 183 (1991) 217

[7] Albertini, G., R. Coppola, Nucl. Instr. Meth. A 314 (1992) 352

[8] Phytian, W.J., A.J.E. Foreman, C.A. English, J.T. Buswell, M. Hetherington, K. Roberts, S. Pizzini, „The Structure and Hardening Mechanism of Copper Precipitation in Thermally Aged or Irradiated Fe-Cu and Fe-Cu-Ni Model Alloys, in: „Effects of Radiation on Materials", 15th International Symposium, ASTM STP 1125, R.E. Stoller, A.S. Kumar, D.S. Gelles, Eds., 1992, pp. 131-150

[9] Albertini, G., R. Coppola, F. Rustichelli, Phys. Rep. 233 (1993) 137

[10] Solt, G., W.B. Waeber, F. Frisius, U. Zimmermann, Materials Science Form 97-99 (1992) 273-298

[11] Brauer, G., F. Eichhorn, F. Frisius, R. Kampmann: „Investigation of Neutron Irradiated Soviet-Type Reactor Pressure Vessel Steels by Small Angle Neutron Scattering", in: Effects of Radiation on Materials: 16th International Symposium, ASTM STP 1175, A.S. Kumar, D.S. Gelles, R.K. Nanstad, E.A. Little, Eds. 1993, pp. 503-515

[12] Buswell, J.T., C.J. Bolton, M.R. Woolton, P. Bischler, J.E. Jones, R.B. Jones, W.J. Phytian, R.N. Sinclair, „The Radiation Hardening and Embrittlement of a Mild Steel Submerged-Arc Weld", in: Effects of Radiation on Materials: 16th International Symposium, ASTM STP 1175, A.S. Kumar, D.S. Gelles, R.K. Nanstad, E.A. Little, Eds. 1993, pp. 332-351

[13] Solt, G., F. Frisius, W.B. Waeber, P. Tipping, „Irradiation-Induced Precipitation in Modell Alloys with Systematic Variation of Cu, Ni, and P content: A Small Angle Neutron Study", in: Effects of Radiation on Materials: 16th International Symposium, ASTM STP 1175, A.S. Kumar, D.S. Gelles, R.K. Nanstad, E.A. Little, Eds. 1993, pp. 444-461

[14] Williams, T.J., W.J. Phythian, „Electron Microscopy and Small Angle Neutron Scattering Study of Precipitation in Low Alloy Steel Submerged - Arc Welds", in: „Effects of Radiation on Materials: 17th International Symposium, ASTM STP 1270, D.S. Gelles, R.K. Nanstad, A.S. Kumar, E.A. Little, Eds., 1996, pp. 191-205

[15] Albertini, G., F. Carsughi, R. Coppola, F. Rustichelli, M. Stefanon, „Radiation Damage Studies Using Small-Angle Neutron Scattering", in: „Effects of Radiation on Materials: 17th International Symposium, ASTM STP 1270, D.S. Gelles, R.K. Nanstad, A.S. Kumar, E.A. Little, Eds., 1996, pp. 206-219

[16] Große, M., F. Eichhorn, J. Böhmert, G. Brauer, „Characterization of Irradiation-induced Precipitates by Small Angle X-ray and Neutron Scattering Experiments, in: „Effects of Radiation on Materials: 17th International Symposium, ASTM STP 1270, D.S. Gelles, R.K. Nanstad, A.S. Kumar, E.A. Little, Eds., 1996, pp. 1123-1133

[17] Albertini, G., F. Garsughi, R. Coppola, F. Fiori, F. Rusichelly, M. Stefanon, J. Nucl. Mater. 233-237 (1996) 253-257

[18] Buswell, J.T., W.J. Phythian, R.J. McElroy, S. Dumbill, R.H.N. Ray, J. Mace, R.N. Sinclair, J. Nucl. Mater. 225 (1995) 196-214

[19] Wirth, B.D., G.R. Odette, W.A. Pavinich, G.E. Lucas, S.E. Spooner, „Small Angle Neutron Scattering Study of Linde 80 RPV Welds", in: „Effects of Radiation on Materials: 18th International Symposium, ASTM STP 1325, R.K. Nanstad, M.L. Hamilton, F.A.. Garner, A.S. Kumar, Eds., 1999, pp. 102-121

[20] Sokolev, M.A., S. Spooner, G.R. Odette, B.D. Wirth, G.E. Lucas, „SANS Study of High Copper RPV Welds in Irradiated and Annealed Conditions, in: „Effects of Radiation on Materials: 18th International Symposium, ASTM STP 1325, R.K. Nanstad, M.L. Hamilton, F.A.. Garner, A.S. Kumar, Eds., 1999, pp. 333-345

[21] Große, M., P. Nitzsche, J. Böhmert, G. Brauer, „Investigation of the Development of Irradiation-Induced Precipitates in VVER-440-type Reactor Pressure Vessel Steels and Weld Metals after Irradiation and Annealing, in: „Effects of Radiation on Materials: 18th International Symposium, ASTM STP 1325, R.K. Nanstad, M.L. Hamilton, F.A.. Garner, A.S. Kumar, Eds., 1999, pp. 346-362

[22] Böhmert, J.,M. Große, Nachweis von Bestrahlungsdefekten in WWER-RDB-Stählen durch Kleinwinkelstreuexperimente
Jahrestagung Kerntechnik 1995, Tagungsbericht, Bonn, Mai 1995, S. 379-383

[23] Große, M., F. Eichhorn, J. Böhmert, H.-G. Haubold, G. Goerigk, ASAXS and SANS Investigations of the Chemical Composition of Irradiation-Induced Precipitates in Nuclear Pressure Vessel Steels, Nucl. Instruments and Methods in Physics Research B97 (1995) 487-490

[24] Große, M., A. Hempel, J. Böhmert, G. Brauer, F.H. Haggag, Influence of the Irradiation Temperature on the Formation of Defects in Reactor Pressure Vessel Steels, MRS 1996 Fall Meeting, Dez. 1996, Boston (Mass.), Proc.

[25] Böhmert, J., M. Große, P. Nitzsche, SANS investigations of the irradiation-caused structural damages in VVER 440-type reactor pressure vessel steels Physica B 234-236 (1997) 997-998

[26] Böhmert, J., M. Große, Nanoscale Precipitates in Russian Reactor Pressure Vessel Steel After Irradiation and Annealing, Jahrestagung Kerntechnik 1998, 26.-28. Mai 1998, Tagungsbericht, München, S. 741

[27] Große, M., J. Böhmert, R. Gilles, Small angle neutron scattering investigations of the microstructure of VVER-440-type reactor pressure vessel steel after irradiation at 60 °C, Journal of Nuclear Materials, Vol. 254 (1998) 143 -150

[28] Große, M., V. Denner, J. Böhmert, Irradiation-Induced Structural Changes in Surveillance Material of the VVER-440-type Weld Metal Sr-10KhMFT, J. Nucl. Mater., Vol. 277 (2000) 280-287

[29] Vonk, C.G., J. Appl. Cryst. (1976) 9, 433-440

[30] Glatter, O., J. Appl. Cryst. (1980) 13, 7-11

[31] Potton, J.A., G.J. Daniell, B.D. Rainford, J. Appl. Cryst. 21 (1988) 663

[32] Potton, J.A., G.J. Daniell, B.D. Rainford, J. Appl. Cryst. 21 (1988) 891

[33] Magnani, M., P. Puliti, M. Stefonon, Nucl. Instr. Meth. A 271 (1988) 611

[34] Frisius, F., R. Kampmann, P.A. Breaven, R. Wagner, Proc., BNES Conf. „Dimensional Stability and Mechanical Behaviour of Irradiated Metals and Alloys", Vol. 1, London, 1983, p. 171

[35] Große, M., A. Gokhman, J. Böhmert, Nucl. Instr. and Methods B, submitted

[36] Böhmert, J., A. Kryukov, Yu.A. Nikolaev, Yu.N. Korolev, D.Yu. Erak, S.S. Gerashenko, Einfluß der Zusammensetzung auf die Strahlenversprödung von Eisenlegierungen, Forschungszentrum Rossendorf, FZR-255, Feb. 1999

[37] Kostorz, G., S.W. Lovesey, Neutron Scattering - General Introduction, in: Treatise on Materials Science and Technology, Vol. 15, Neutron Scattering, G. Kostorz, Ed., New York, 1979, pp. 2-67

[38] Saltykov, S.A., Sterometrische Metallographie, Deutscher Verlag d. Grundstoffindustrie, 1. Auflage, Leipzig, 1974, S. 283

[39] Doherly, R.D., „Diffusive Phase Transformation in the Solid State", Chapter 14 in R.W. Cahn, P. Haasen, eds., „Physical Metallurgy", third edition, Elsevier Science Publishers, 1983

[40] Fegin, L.A., D.I. Svergun, „Structure Analysis by Small-Angle X-Ray and Neutron Scattering", Plenum Press N.Y., pp. 335

[41] Kontsky, J, J. Kocik, „Radiation Damage of Structural Materials", Academic Prague, 1994

[42] Ulbricht, A., J. Böhmert, SANS experiments at iron test alloys, paper on Jahrestagung Kerntechnik 2000, submitted

[43] Pareige, P., R.E. Stoller, K.F. Rusell, M.K. Miller, J. Nucl. Mat. 1997 (249) 165-176

[44] Orowan, E., Dislocation in Metals, AIME, p. 131

[45] Friedel, J., „Dislocations" Pergamon Press, N.Y.

[46] Week, R.W., S.R. Pati, M.F. Asby, P. Barrand, Acta Met. 17 (1990) 1403-1410

[47] Russell, K.C., L.M. Brown, Acta Met. 20 (1972) 969-974

[48] Kojima, S., S.J. Zinkle, H.L. Heinrich, Journal of Nucl. Mat. 179-181 [1991] 982-985

[49] Stoller, R.E., „Pressure Vessel Embrittlement Predictions Based on a Composite Model of Copper Precipitation and Point Defect Clustering", Effects of Radiation on Materials: 17th International Symposium, ASTM STP 1270, D.S. Gelles, R.K. Nanstad, A.S. Kumal, E.A. Little, Eds. American Society for Testing and Materials, 1996, pp. 25-58

[50] Brown, L.M., R.K. Ham, „Strengthening Methods in Crystals", A. Kelly, R.B. Nicholson (eds.), 1971, p. 12

Annex

Description of the Programme System FPM-99

A. Gokhman

Programme system FPM-99 realizes a method to find the parameters of the size distribution functions (SDF) in a structure consisting of two different types of scattering particles embedded in a homogeneous matrix from small angle magnetic or nuclear scattering data. Log normal functions are used as the basic functions.

The parameters of the log normal functions are found from the condition of minimal differences between experimental scattering data and the data recalculated from fit SDF. Each experimental value has an own statistical weight that is inverse proportional to the relative experimental error of it. The direct way to found the fit parameters is used: both linear parameters change from 0.1 till 10.5 nm with steps of 0.01 nm; the range of changing of the relative content of particles depends on the damage structure given.

At the first step the fit parameters of the normalized log normal functions and the relative content of particles are found from the condition of minimal difference between normalized experimental and recalculated scattering data. At the second step the volume content and mean R-value of the both phases are calculated.

FPM-99 is worked out on FORTRAN for IBM-PCI.

Input data:

- Experimental small angle magnetic or nuclear scattering experimental intensity and its error as a function of the magnitude of scattering vector,
- A-ratio of the both types of particles,
- Bessel function of the first order with steps of 0.01.

Output data:

- Parameters of the SDF of the first type and the second type of particles,
- Thickness of the cylinder for cylindrical type of precipitates,
- SDF of the both particle types and total SDF,
- Normalized experimental small angle scattering intensity and normalized small angle scattering intensity recalculated from SDF,
- Volume content of both particle types,
- Mean radius of each particle type and total mean radius.

Texts of programmes are given in directory:

Gokhman-Fitpar-Text of Programs

Programme GTM. For realizes fit parameters method for two-type spherical damage structure if magnetic scattering data are used;

Programme GTN. For realizes fit parameters method for two-type spherical damage structure if nuclear scattering data are used;

Programmes **CTAB1. For, CTAB2. For, CTBB1. For, CTGB2. For and CTHB2. For** realize the fit parameters in case, when one type of particles has cylindrical shape with arbitrary ratio between length and radius of them and the other type has a spherical shape.

Input and the output data can be transformed in graphics by means of Excel.